




# Theoretical and Computational Analysis at a Quantum State Level of Autoionization Processes in Astrochemistry

Stefano Falcinelli<sup>1</sup> , Fernando Pirani<sup>2,3</sup>, Marzio Rosi<sup>1,3</sup>,  
and Franco Vecchiocattivi<sup>1</sup>

- <sup>1</sup> Department of Civil and Environmental Engineering, University of Perugia,  
Via G. Duranti 93, 06125 Perugia, Italy  
{stefano.falcinelli,marzio.rosi}@unipg.it,  
franco@vecchio.it
- <sup>2</sup> Department of Chemistry, Biology and Biotechnologies, University of Perugia,  
Via Elce di Sotto 8, 06100 Perugia, Italy  
fernando.pirani@unipg.it
- <sup>3</sup> ISTM-CNR, 06123 Perugia, Italy

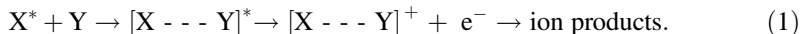
**Abstract.** Changes in atomic-molecular alignment and/or in molecular orientation, can affect strongly the fate of basic collision events. However, a deep knowledge of these phenomena is still today not fully understood, although it is of general relevance for the control of the stereo-dynamics of elementary chemical-physical processes, occurring under a variety of conditions, both in gas phase and at surface. In particular, understanding the mode-specificity in reaction dynamics of open-shell atoms, free radicals, molecules, atomic and molecular ions, under hyper-thermal, thermal and sub-thermal conditions is of fundamental importance for catalysis, plasmas, photo-dynamics as well as interstellar and low-temperature chemistry. In this paper recent results on the role of atomic alignment effects on the stereo-dynamics of autoionization reactions are presented and discussed.

**Keywords:** Autoionization · Stereo-dynamics · State to state · Charge transfer · Transition state · Electron spectroscopy · Astrochemistry

## 1 Introduction

The knowledge of strength, anisotropy and radial dependence of the leading intermolecular interaction components is a crucial objective to assess the selectivity of the molecular dynamics under a variety of conditions. The charge transfer (CT), a basic component of the intermolecular interaction, whose role is often not fully understood, affects myriad of phenomena, including also the formation of intermolecular halogen and hydrogen bonds [1–3].

The focus of this paper is to point out a theoretical and computational methodology based on the selective role of anisotropic CT on the stereo-dynamics of autoionization processes, also known as Penning or chemi-ionization phenomena [4, 5]. Such elementary reactions can be represented according to Eq. (1) below:



In Eq. (1),  $X^*$  is a metastable excited species inducing ionization of a collisional target  $Y$  that can be an atom or a molecule;  $[X \dots Y]^*$  and  $[X \dots Y]^+$  are the intermediate neutral and ionic collisional complexes, respectively, being the first the transition state of the reaction [6, 7]. In general,  $X^*$  species that can be used to induce autoionization are the rare gas atoms in their first excited electronic level which is characterized by a high excitation energy and a considerably long lifetime (see Table 1 below [4, 8]).

**Table 1.** Metastable noble-gas atoms and their fundamental properties [4, 8].

Metastable species	Electronic configuration	Lifetime (s)	Energy (eV)
He <sup>*</sup> (2 <sup>1</sup> S <sub>0</sub> )	1s 2s	0.0196	20.6158
He <sup>*</sup> (2 <sup>3</sup> S <sub>1</sub> )	1s 2s	9000	19.8196
Ne <sup>*</sup> ( <sup>3</sup> P <sub>0</sub> )	2p <sup>5</sup> 3s	430	16.7154
Ne <sup>*</sup> ( <sup>3</sup> P <sub>2</sub> )	2p <sup>5</sup> 3s	24.4	16.6191
Ar <sup>*</sup> ( <sup>3</sup> P <sub>0</sub> )	3p <sup>5</sup> 4s	44.9	11.7232
Ar <sup>*</sup> ( <sup>3</sup> P <sub>2</sub> )	3p <sup>5</sup> 4s	55.9	11.5484
Kr <sup>*</sup> ( <sup>3</sup> P <sub>0</sub> )	4p <sup>5</sup> 5s	0.49	10.5624
Kr <sup>*</sup> ( <sup>3</sup> P <sub>2</sub> )	4p <sup>5</sup> 5s	85.1	9.9152
Xe <sup>*</sup> ( <sup>3</sup> P <sub>0</sub> )	5p <sup>5</sup> 6s	0.078	9.4472
Xe <sup>*</sup> ( <sup>3</sup> P <sub>2</sub> )	5p <sup>5</sup> 6s	150	8.3153

As clearly indicated by the data reported in Table 1, the autoionization reactions are promoted by collisions of an open shell atom, electronically excited in a high energetic metastable state, with another atomic/molecular partner giving rise to the spontaneous emission of electrons accompanied by the formation of parent ions, aggregate ions and fragmentation ions. Therefore, the measure of the energy dependence of emitted electrons, also known as Penning Ionization Electron Spectra (PIES), provides direct information on the electronic rearrangements occurring within the collision complex, which directly correlates with the transition state of the autoionization processes. Moreover, molecular ionization probability and emitted PIES are strongly dependent on symmetry and energy of the atomic or molecular orbital from which the electron is extracted and then on their spatial orientation within the collision complex [7, 9].

Autoionization processes represent also barrier-less reactions, driven by an anisotropic optical potential (see next section), whose real part controls approach of reactants and removing of products, while the imaginary part triggers the passage from neutral reactants to ionic products through an electronic rearrangement. The investigation of these reactions is important for fundamental researches, to assess the coherent control of reactive events at low temperature and then to explore the quantum nature of matter [10]. Autoionization reactions are of interest in radiation and plasma chemistry [11, 12], for the development of excimer lasers and in combustion chemistry [13–15]. More recently, they attracted the attention of the scientific community since they can be involved in the chemistry of planetary ionospheres as well as in astrochemistry [16–24]. These processes can be studied in laboratory using various techniques employing the molecular beam method in high vacuum apparatuses able to detect reactive events in a single-collision condition [25–27]. The main diagnostic experimental procedures are the mass spectrometry [28–31] and the electron spectroscopy [32, 33] coupled with either ion-imaging [34, 35] and coincidence techniques [36, 37]. All these techniques are available in our laboratory.

The Fig. 1 shows a schematic view of the molecular beam apparatus operating in our laboratory (briefly presented in the Sect. 3) and depicts a metastable  $\text{Ne}^*$  atom, whose external electron is excited in the 3s orbital and its ionic core exhibits the same electronic configuration of the high electron affinity fluorine atom, that approaches to a water molecule [33]. This event originates a collision complex where the spontaneous electron jumps from one of HOMO orbitals of water to the ionic core of  $\text{Ne}^*$  and releases enough energy to eject the 3s electron with a defined kinetic energy. Therefore, the measure of the energy dependence of emitted electrons by PIES experiments provides a direct characterization of the transition state of the autoionization reaction (i.e. symmetry and energy of the involved molecular orbitals and the spatial molecular orientation within the collision complex, as depicted in Fig. 1). We characterized in details such features for important hydrogenated molecules, as water, ammonia and hydrogen sulfide, and obtained results have been reported in previous published papers [7, 9, 33, 38].

However, the dependence of the reaction probability on the valence orbital alignment of open-shell atoms still represents a basic open question. Recently [39, 40], our investigation has been focused on some prototype atom-atom reactions, as that involving  $\text{Ne}^* - \text{Kr}$ , in order to obtain information on this basic target. New insights on the stereo-dynamics of elementary processes involved are presented and discussed in the next section.

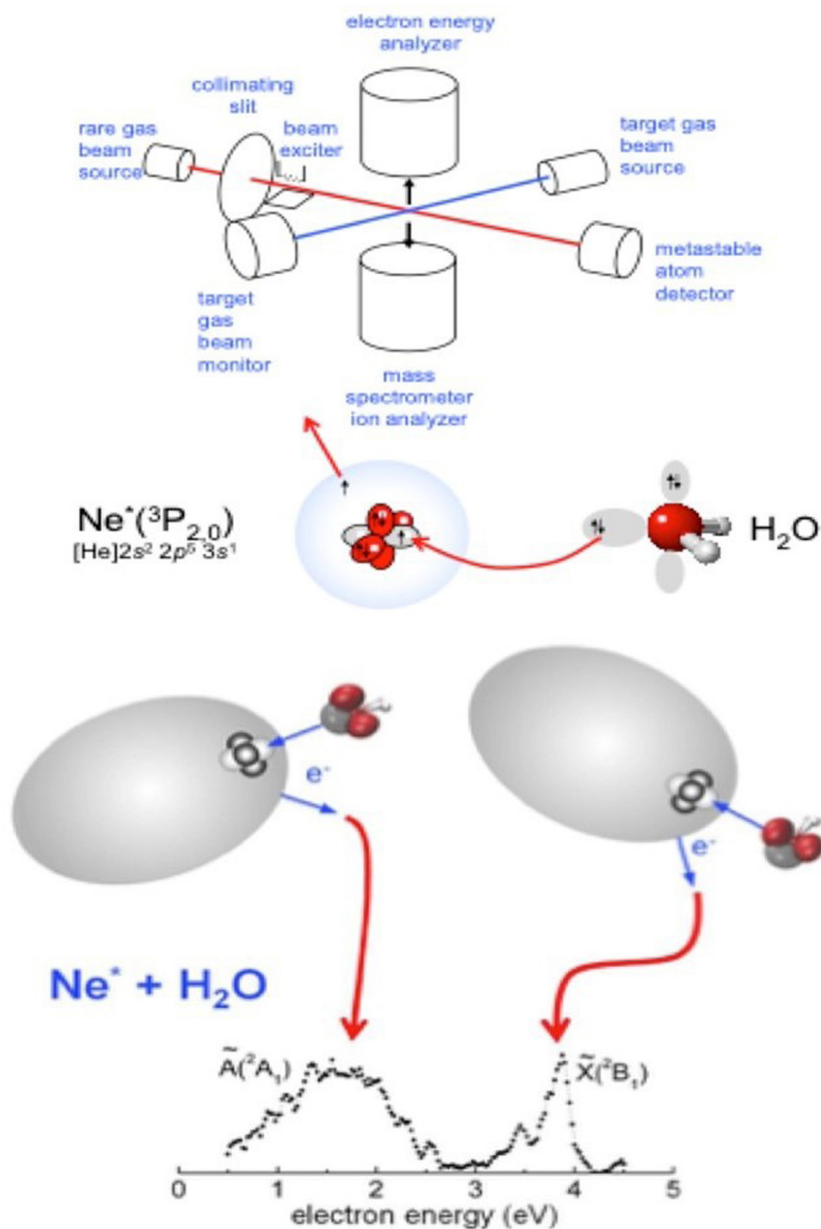


**Fig. 1.** - *Upper panel:* A schematic view of the apparatus, where the primary beam of  $Ne^*(^3P_{2,0})$  atoms, emerging from an electron bombardment supersonic seeded source, crosses at right angles the secondary beam of  $H_2O$  molecules. PIES have been measured exploiting a hemispherical electron energy analyzer, while total, partial cross sections and branching ratios have been determined by the mass spectrometry technique. - *Middle panel:* A scheme of the atomic and molecular orbitals involved in the electron exchange. - *Lower panel:* A scheme of two different transition states leading to the formation of water ion in ground and excited states with the associated PIES [33, 38].

## 2 The Theoretical and Computational Approach

From a theoretical point of view, autoionization reactions are represented employing the so called optical potential model first introduced by Bethe in 1940 [41], which is based on a complex potential  $W$ , according to Eq. (2):

$$W = V - \frac{i}{2} \Gamma \tag{2}$$

Where  $V$  is the real part  $V$  describing the  $X^* + Y$  collision and the relative interaction while  $\Gamma$  represents the imaginary part of such a complex potential accounting for the probability of the electron ejection from the intermediate collisional complex  $[X - - - Y]^*$ , i.e. the transition state of the reaction (see Eq. (1)) [42–44].

In our theoretical approach, the two  $V$  and  $\Gamma$  components are, for the first time, considered as interdependent [5, 45], whose magnitude is related to the internuclear distance,  $R$ , between  $X$  and  $Y$ , their relative orientation and the manifold of quantum states attainable for the system along the collision.

In the description of the autoionization event induced by the  $X^*+Y$  collision, the lifetime,  $\tau$ , of the intermediate autoionizing complex  $[X - - - Y]^*$  is depending on the internuclear distance  $R$ , and is given by the following simple equation:

$$\tau(R) = \frac{\hbar}{\Gamma(R)} \tag{3}$$

Along the element  $dR$ , at the distance  $R$ , during a collision with asymptotic speed  $g$  and a collision energy  $E$ , with impact parameter  $b$ , the probability that the system ionizes is given by

$$P(R)dR = \frac{\Gamma(R)}{\hbar g \left[1 - \frac{V(R)}{E} - \frac{b^2}{R^2}\right]^{\frac{1}{2}}} dR \tag{4}$$

During a complete collision, the probability that the system survives (i.e. does not give rise to ionization) from infinite distance to the turning point  $R_c$  is:

$$F_{R_c, \infty}(b, g) = \exp \left[ - \int_{R_c}^{\infty} P(R) dR \right] = \exp \left[ - \int_{R_c}^{\infty} \frac{\Gamma(R)}{\hbar g \left[1 - \frac{V(R)}{E} - \frac{b^2}{R^2}\right]^{\frac{1}{2}}} dR \right] \tag{5}$$

The total ionization cross section will be given by:

$$\sigma_{tot}(g) = 2\pi \int_0^{\infty} P(b) b db = 2\pi \int_0^{\infty} \left[ 1 - F_{R_c, \infty}^2(b, g) \right] b db \tag{6}$$

For associative ionization, it is necessary to define the limit distance,  $R_{ass}$ , above which associative ionization (i.e. the formation of the  $XY^+$  molecular ion) cannot take place. If  $V_{in}(R)$  is the input potential (describing the incoming collision between the neutral  $X^*+Y$  partners) and  $V_{out}(R)$  is the output potential (accounting for the interaction between the separating products  $X+Y^+$ ),  $R_{ass}$  is defined by the condition:

$$V_{in}(R_{ass}) - E = V_{out}(R_{ass}) - H \quad (7)$$

where  $H$  is the height of the centrifugal barrier, i.e. the maximum of the following function:

$$\frac{Eb^2}{R_{ass}^2} \quad (8)$$

The probability of associative ionization is given by:

$$P_{ass}(b, g) = F_{R_{ass}, \infty} \left[ 1 - F_{R_{c, ass}}^2(b, g) \right] \quad (9)$$

from which the cross section for associative ionization is obtained

$$\sigma_{ass}(g) = 2\pi \int_0^{\infty} P_{ass}(b) b db = 2\pi \int_0^{\infty} F_{R_{ass}, \infty} \left[ 1 - F_{R_{c, ass}}^2(b, g) \right] b db \quad (10)$$

### 3 Results and Discussion

The experimental devices used to investigate the dynamics of the autoionization reaction involving metastable atoms and using mass spectrometry, electron spectroscopy, ion-imaging and coincidence techniques has been presented in details in previous papers [46–50] and a schematic view is given in the upper part of Fig. 1.

Shortly, it is a molecular beam (MB) apparatus, formed by a noble gas beam source from which the emerging Ne atoms are electronically excited by collisions with energetic electrons. The  $Ne^*$  MB crosses at right angles the MB of target species, which in recent experiments are noble gas atoms. PIES are measured by exploiting an hemispherical electron energy analyzer, while total, partial ionization cross sections and branching ratios (BRs), with their collision energy dependence, are obtained exploiting the mass spectrometry technique. In the present case, BRs of relevance are also those associated to the relative formation probability of the *parent ion*  $Kr^+$  and of the ionic adduct  $Kr^+ - Ne$ , also indicated as *associated ion*.

Results of recent experiments [39, 40, 46], performed at low collision energy and under high resolution conditions, permitted us to separate in measured PIES (left panel in Fig. 2) the contributions of entrance and exit channels referred to specific spin-orbit levels of  $Ne^*$  reagent and of  $Kr^+$  product, which are both open shell species. Moreover, PIES have been also measured as a function of the collision energy and obtained results are plotted in the right panel of Fig. 2.

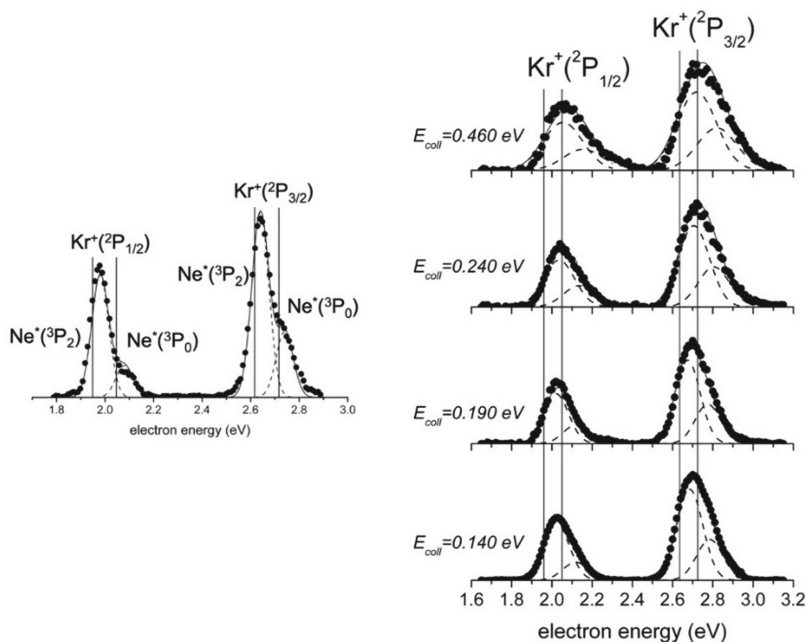


**Fig. 2.** *Left panel:* A  $\text{Ne}^*$  - Kr PIES measured at low collision energy (50 meV), where the contributions of four reaction channels, associated to two different spin-orbit states  $J$  of  $\text{Ne}^*$  neutral reactant ( $J_i = 2, 0$ ) and of  $\text{Kr}^+$  ionic product ( $J_f = 3/2, 1/2$ ), have been resolved. Vertical continuous lines represent the peak positions as predicted for the ionization of Kr by Ne(I) photons, and the shift of observed maxima in measured PIES relates to structure and stability of the reaction transition state [39]. The peak area ratios, defining the relative reaction yields of the four channels, have been also evaluated through the analysis performed adopting four independent Gaussian functions with the same width [39, 40]; *Right panel:* PIESs measured as a function of the collision energy (vertical lines as in the left lower panel). Their analysis emphasizes the dependence of the peak position and of the peak area ratios on the collision energy.

Their analysis provided the dependences on the collision energy of the peak positions, related to the change of the transition state stability, and of the peak area ratios, determined by the change of relative reaction yields. These experimental findings, coupled with the ample phenomenology achieved in our laboratory on the anisotropic dynamical behavior of open-shell atoms [51, 52], suggested us that electronic rearrangements driving the reaction directly arise from polarization of external-floppy cloud of the 3s electron, charge transfer and modifications of angular momentum couplings of other valence electrons within the collision complex. Such rearrangements are accompanied by *adiabatic* and *non-adiabatic effects*, which play a crucial role in the control of the collision dynamics.

In particular, *adiabatic effects* mostly arise from strength and selectivity of configuration interaction which couples entrance,  $V_{in}$ , and exit,  $V_{out}$ , channels, having the same molecular symmetry and differing for one electron exchange. They affect the

anisotropic behavior of the real part,  $V$ , of the optical potential (see Eq. (2)) and account for the adiabatic conversion of atomic states, defined in terms of  $|J, \Omega\rangle$  quantum numbers, where  $J$  represents the total electronic angular momentum of open shell species and  $\Omega$  describes its projection along the interatomic direction, into molecular states of  $\Sigma$  and  $\Pi$  symmetry. The latter are emerging only at short separation distances, while the atomic states are representative of the system at large distances. Moreover, this conversion involves both entrance and exit channels and obtained interaction components.

The imaginary  $\Gamma$  components (see Eq. (2)), defined in terms of quantum numbers proper of entrance and exit channels, are controlled by strength and radial dependence of *non-adiabatic effects*. They arise again from polarization, selective configuration interactions, changes in electron angular momentum couplings, spin-orbit and Coriolis contributions.

The nature of the *non-adiabatic effects* suggests that the autoionization reaction occurs through two complementary microscopic mechanisms, as discussed in recent papers [39, 40]:

They are classified as:

- i) *direct mechanism* - it is triggered by a homogeneous electron exchange, with coupling terms, between entrance and exit channels, called  $A_{\Sigma-\Sigma}$  and  $A_{\Pi-\Pi}$  on the basis of molecular character ( $\Sigma$  or  $\Pi$ ) of initial and final state;
- ii) *indirect mechanism* - it is stimulated by a heterogeneous electron exchange and it is accompanied by mixing/exchange between initial and final states of different symmetry. Such mechanism is basically promoted by spin-orbit and Coriolis coupling effects.

It is important to note that the two mechanisms show a different radial dependence and therefore their relative role varies with the collision energy as previously discussed [39, 40].

The interaction components, formulated as summarized above and published in recent papers [45, 53], permitted us to calculate within the semiclassical method outlined in Sect. 3, the total ionization cross sections in a wide collision energy range for three investigated  $\text{Ne}^* - \text{Ng}$  (where  $\text{Ng} = \text{Ar}, \text{Kr}$  and  $\text{Xe}$ ) autoionization systems. Obtained results are plotted in Fig. 3. Using this methodology, we were able also to calculate branching ratios (BRs) between selected reaction channels (see Eq. (11) below). This provided an internally consistent rationalization of most relevant experimental findings, characterized with different techniques in various laboratories, that includes total and partial ionization cross sections, BRs and PIES measurements [53–56]. The energy dependence of BRs between selected reaction channels must also relate with the PIES spectra for  $\text{Ne}^* - \text{Ng}$  systems measured in our laboratory [5, 39, 40] as those reported in Fig. 2 where, as an example, are showed only those for  $\text{Ne}^* - \text{Kr}$ .

The PIES spectra of  $\text{Ne}^* - \text{Ng}$  are composed of 4 peaks, and each of relative area  $R_A, R_B, R_C, R_D$  are evaluated according to the scheme of Fig. 4, and according to the following equations:



$$R_A = \frac{Q_{2-3/2}}{Q_{0-3/2}}; R_B = \frac{Q_{0-1/2}}{Q_{0-3/2}}; R_C = \frac{Q_{2-1/2}}{Q_{0-3/2}}; R_D = \frac{Q_{2-1/2}}{Q_{2-3/2}} \quad (11)$$

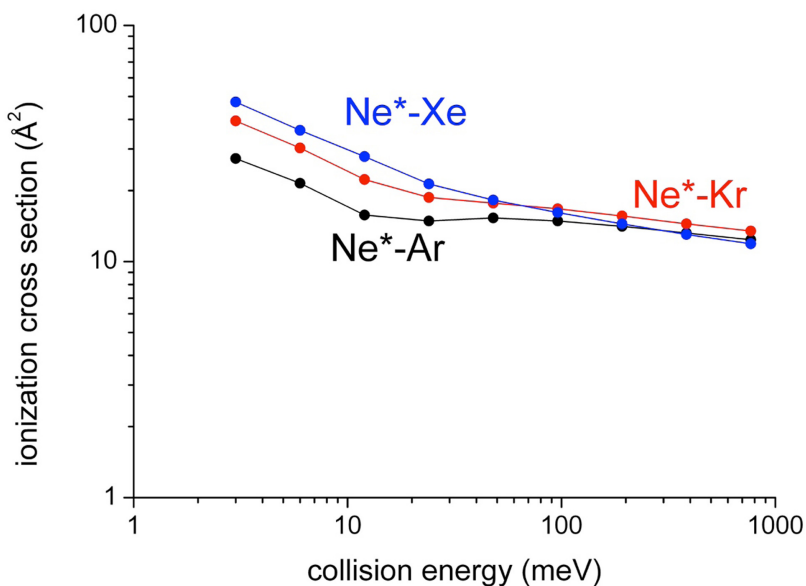


**Fig. 3.** The total ionization cross sections calculated by the semiclassical method outlined in Sect. 3 for Ne\* - Xe (points and blue line), Ne\* - Kr (points and red line) and Ne\* - Ar (points and black line). (Color figure online)

$$\begin{array}{l}
 \left. \begin{array}{l} 2P_{1/2} \\ 2P_{3/2} \end{array} \right\} \begin{array}{l} Q_{0-1/2} = \sigma_{00-1/2,1/2} \\ Q_{0-3/2} = \sigma_{00-3/2,1/2} + \sigma_{00-3/2,3/2} \end{array} \\
 3P_0 \\
 \\
 \left. \begin{array}{l} 2P_{1/2} \\ 2P_{3/2} \end{array} \right\} \begin{array}{l} Q_{2-1/2} = \sigma_{20-1/2,1/2} + 2\sigma_{21-1/2,1/2} + 2\sigma_{22-1/2,1/2} \\ Q_{2-3/2} = \sigma_{20-3/2,1/2} + \sigma_{20-3/2,3/2} + 2\sigma_{21-3/2,1/2} \\ \quad + 2\sigma_{21-3/2,3/2} + 2\sigma_{22-3/2,1/2} + 2\sigma_{22-3/2,3/2} \end{array} \\
 3P_2
 \end{array}$$

**Fig. 4.** The scheme used for the evaluation of the of relative area  $R_A$ ,  $R_B$ ,  $R_C$ ,  $R_D$  in the observed peaks of Ne\* - Ng PIES spectra (see text).

Where the used parameters are defined in Fig. 5.

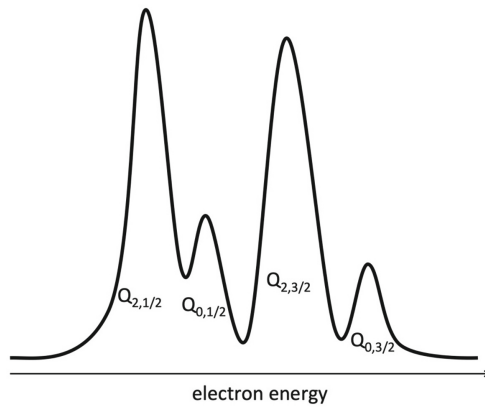


**Fig. 5.** The typical  $\text{Ne}^*$  - Ng PIES spectrum with the definition of parameters used in Eq. (11) (see text).

By analyzing the PIES spectra previously measured in our laboratory (see for example those reported in Fig. 2) [39, 46] we performed cross section ratios calculations of different channels  $|J_i \rightarrow J_f\rangle$  for all  $\text{Ne}^*$  - Ng (Ng = Ar, Kr, and Xe) systems on the basis of the semiclassical treatment discussed in Sect. 3. The obtained data are reported in Figs. 6, 7 and 8 where continuous lines of different colors are the results of the present treatment carried out assuming a  ${}^3\text{P}_2/{}^3\text{P}_0$  population ratio of about 3, as found for a  $\text{Ne}^*$  beam generated by electron impact [33].

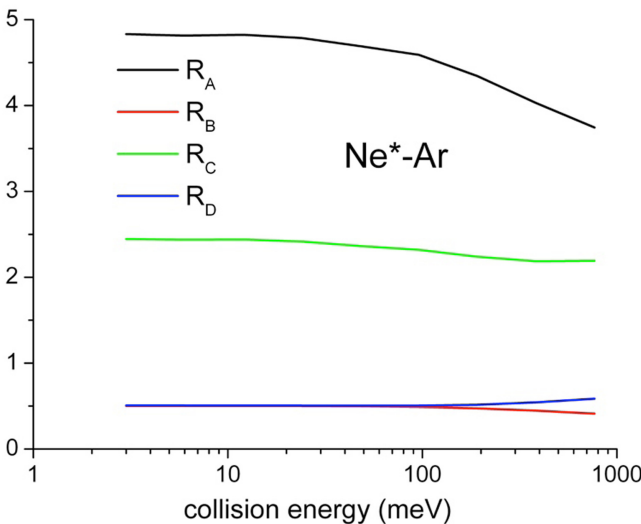


**Fig. 6.** Cross section ratios of different channels  $|J_i \rightarrow J_f\rangle$  calculated for  $\text{Ne}^*$  - Ar system as a function of the collision energy, and analyzing the peak areas obtained in PIES measurements according to Eq. (10) and Figs. 4 and 5. The continuous lines are the results of the present treatment carried out assuming a  ${}^3\text{P}_2/{}^3\text{P}_0$  population ratio of about 3, as found for a  $\text{Ne}^*$  beam generated by electron impact (see text).

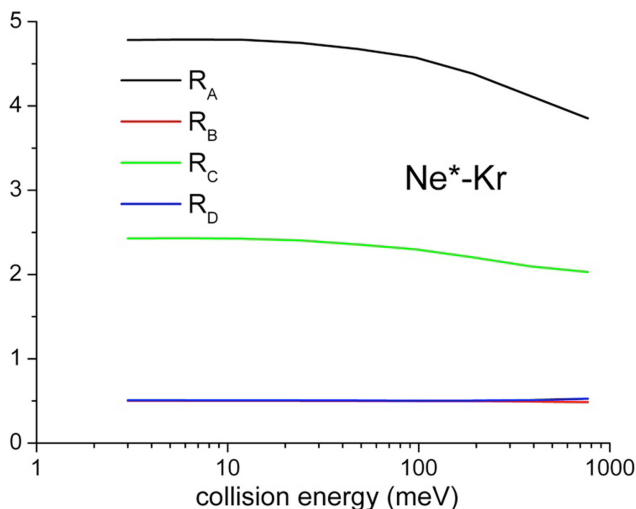


**Fig. 7.** Cross section ratios of different channels  $|J_i \rightarrow J_f\rangle$  calculated for  $\text{Ne}^* - \text{Kr}$  system as a function of the collision energy, and analyzing the peak areas obtained in PIES measurements according to Eq. (10) and Figs. 4 and 5. The continuous lines are the results of the present treatment carried out assuming a  ${}^3\text{P}_2/{}^3\text{P}_0$  population ratio of about 3, as found for a  $\text{Ne}^*$  beam generated by electron impact (see text). In the figure the red line of  $R_B$  cross section ratio is not visible since superimposed by the blue ones related to  $R_D$ . (Color figure online)

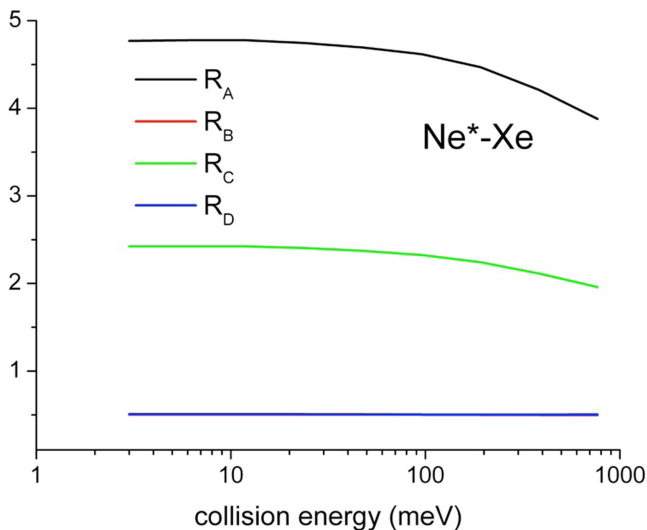


**Fig. 8.** Cross section ratios of different channels  $|J_i \rightarrow J_f\rangle$  calculated for  $\text{Ne}^* - \text{Xe}$  system as a function of the collision energy, and analyzing the peak areas obtained in PIES measurements according to Eq. (10) and Figs. 4 and 5. The continuous lines are the results of the present treatment carried out assuming a  ${}^3\text{P}_2/{}^3\text{P}_0$  population ratio of about 3, as found for a  $\text{Ne}^*$  beam generated by electron impact (see text). In the figure the red line of  $R_B$  cross section ratio is not visible since superimposed by the blue ones related to  $R_D$ . (Color figure online)

## 4 Conclusions

In conclusion, the discussed methodology provides unique information on the stereodynamics of autoionization reactions. In this paper it is applied to prototype  $\text{Ne}^* - \text{Ng}$  atom-atom systems, and allows to rationalize in a unifying picture most of the available experimental findings from our and other laboratories. This opened the possibility to obtain *state to state* cross sections which is of great interest for the investigation of quantum effects in the coherent control of collision processes in astrochemistry, promoting Penning and associative ionization, from ultra-cold up to thermal reactive collisions [10, 57, 58]. Obtained results suggest also how to extend the methodology to autoionization reactions involving molecules [7, 9, 59], which are of great interest in several fields, including the balance of phenomena occurring in interstellar environments and planetary atmospheres. In addition, also electron-molecule impacts are of crucial relevance in many applications of molecular plasmas [5].

**Acknowledgments.** This work was supported and financed with the “Fondo Ricerca di Base, 2018, dell’Università degli Studi di Perugia” (Project Titled: Indagini teoriche e sperimentali sulla reattività di sistemi di interesse astrochimico). Support from Italian MIUR and University of Perugia (Italy) is acknowledged within the program “Dipartimenti di Eccellenza 2018–2022”.

## References

1. Bartocci, A., Belpassi, L., Cappelletti, D., Falcinelli, S., et al.: Catching the role of anisotropic electronic distribution and charge transfer in halogen bonded complexes of noble gases. *J. Chem. Phys.* **142**(18), 184304 (2015)
2. Cappelletti, D., Bartocci, A., Grandinetti, F., Falcinelli, S., et al.: *Chem. Eur. J.* **21**(16), 6234–6240 (2015)
3. Pirani, F., Cappelletti, D., Falcinelli, S., Cesario, D., Nunzi, F., Belpassi, L., Tarantelli, F.: *Angew. Chem. Int. Ed.* **58**(13), 4195–4199 (2019)
4. Siska, P.E.: *Rev. Mod. Phys.* **65**, 337–412 (1993)
5. Falcinelli, S., Pirani, F., Candori, P., Brunetti, B.G., Farrar, J.M., Vecchiocattivi, F.: *Front. Chem.* **7**, 445 (2019)
6. Benz, A., Morgner, H.: *Mol. Phys.* **57**, 319–336 (1986)
7. Falcinelli, S., Bartocci, A., Cavalli, S., Pirani, F., Vecchiocattivi, F.: *Chem. Eur. J.* **22**(2), 764–771 (2016)
8. Falcinelli, S., et al.: Modeling the intermolecular interactions and characterization of the dynamics of collisional autoionization processes. In: Murgante, B., et al. (eds.) *ICCSA 2013*. LNCS, vol. 7971, pp. 69–83. Springer, Heidelberg (2013). [https://doi.org/10.1007/978-3-642-39637-3\\_6](https://doi.org/10.1007/978-3-642-39637-3_6)
9. Falcinelli, S., Rosi, M., Cavalli, S., Pirani, F., Vecchiocattivi, F.: *Chem. Eur. J.* **22**(35), 12518–12526 (2016)
10. Arango, C.A., Shapiro, M., Brumer, P.: *Phys. Rev. Lett.* **97**, 193202 (2006)
11. Falcinelli, S., Capriccioli, A., Pirani, F., Vecchiocattivi, F., Stranges, S., Marti, C., et al.: *Fuel* **209**, 802–811 (2017)
12. Falcinelli, S.: *Catal. Today* **348**, 95–101 (2020)
13. Cavallotti, C., Leonori, F., Balucani, N., Nevrlly, V., Bergeat, A., et al.: *J. Phys. Chem. Lett.* **5**, 4213–4218 (2014)

14. Leonori, F., Balucani, N., Nevrlý, V., Bergeat, A., et al.: *J. Phys. Chem. C* **119**(26), 14632–14652 (2015)
15. Leonori, F., Petrucci, R., Balucani, N., Casavecchia, P., Rosi, M., et al.: *Phys. Chem. Chem. Phys.* **11**(23), 4701–4706 (2009)
16. Rosi, M., Falcinelli, S., Balucani, N., Casavecchia, P., Leonori, F., Skouteris, D.: theoretical study of reactions relevant for atmospheric models of titan: interaction of excited nitrogen atoms with small hydrocarbons. In: Murgante, B., et al. (eds.) *ICCSA 2012. LNCS*, vol. 7333, pp. 331–344. Springer, Heidelberg (2012). [https://doi.org/10.1007/978-3-642-31125-3\\_26](https://doi.org/10.1007/978-3-642-31125-3_26)
17. Alagia, M., Candori, P., Falcinelli, S., Lavollée, M., Pirani, F., Richter, R., Stranges, S., Vecchiocattivi, F.: *Chem. Phys. Lett.* **432**, 398–402 (2006)
18. Alagia, M., Candori, P., Falcinelli, S., Lavollée, M., Pirani, F., Richter, R., Stranges, S., Vecchiocattivi, F.: *J. Phys. Chem. A* **113**, 14755–14759 (2009)
19. Alagia, M., Candori, P., Falcinelli, S., Lavollée, M., Pirani, F., Richter, R., Stranges, S., Vecchiocattivi, F.: *Phys. Chem. Chem. Phys.* **12**, 5389–5395 (2010)
20. Falcinelli, S., Pirani, F., Alagia, M., Schio, L., Richter, R., et al.: *Chem. Phys. Lett.* **666**, 1–6 (2016)
21. Falcinelli, S., Pirani, F., Vecchiocattivi, F.: *Atmosphere* **6**(3), 299–317 (2015)
22. Biondini, F., Brunetti, B.G., Candori, P., De Angelis, F., et al.: *J. Chem. Phys.* **122**(16), 164307 (2005)
23. Biondini, F., Brunetti, B.G., Candori, P., De Angelis, F., et al.: *J. Chem. Phys.* **122**(16), 164308 (2005)
24. Podio, L., Codella, C., Lefloch, B., Balucani, N., Ceccarelli, C., et al.: *MNRAS* **470**(1), L16–L20 (2017)
25. Bartolomei, M., Cappelletti, D., De Petris, G., Rosi, M., et al.: *Phys. Chem. Chem. Phys.* **10**(39), 5993–6001 (2008)
26. Leonori, F., Petrucci, R., Balucani, N., Casavecchia, P., Rosi, et al.: *J. Phys. Chem. A* **113**(16), 4330–4339 (2009)
27. De Petris, G., Cartoni, A., Rosi, M., Barone, V., Puzzarini, C., Troiani, A.: *Chem. Phys. Chem.* **12**(1), 112–115 (2011)
28. Falcinelli, S., Fernandez-Alonso, F., Kalogerakis, K., Zare, R.N.: *Mol. Phys.* **88**(3), 663–672 (1996)
29. Alagia, M., Balucani, N., Candori, P., Falcinelli, S., Richter, et al.: *Rend. Lincei Sci. Fisiche e Naturali* **24**, 53–65 (2013)
30. Ben Arfa, M., Lescop, B., Cherid, M., Brunetti, B., Candori, P., et al.: *Chem. Phys. Lett.* **308**, 71–77 (1999)
31. Brunetti, B.G., Candori, P., Ferramosche, R., Falcinelli, S., et al.: *Chem. Phys. Lett.* **294**, 584–592 (1998)
32. Hotop, H., Illenberger, E., Morgner, H., Niehaus, A.: *Chem. Phys. Lett.* **10**(5), 493–497 (1971)
33. Brunetti, B.G., Candori, P., Cappelletti, D., Falcinelli, S., et al.: *Chem. Phys. Lett.* **539–540**, 19–23 (2012)
34. Falcinelli, S., Rosi, M., Candori, P., Farrar, J.M., Vecchiocattivi, F., et al.: *Planet. Space Sci.* **99**, 149–157 (2014)
35. Pei, L., Carrascosa, E., Yang, N., Falcinelli, S., Farrar, J.M.: *J. Phys. Chem. Lett.* **6**(9), 1684–1689 (2015)
36. Alagia, M., Candori, P., Falcinelli, S., Pirani, F., et al.: *Phys. Chem. Chem. Phys.* **13**(18), 8245–8250 (2011)
37. Alagia, M., Candori, P., Falcinelli, S., Lavollée, M., et al.: *J. Chem. Phys.* **126**(20), 201101 (2007)

38. Balucani, N., Bartocci, A., Brunetti, B., Candori, P., et al.: *Chem. Phys. Lett.* **546**, 34–39 (2012)
39. Falcinelli, S., Vecchiocattivi, F., Pirani, F.: *Phys. Rev. Lett.* **121**(16), 163403 (2018)
40. Falcinelli, S., Vecchiocattivi, F., Pirani, F.: *J. Chem. Phys.* **150**(4), 044305 (2019)
41. Bethe, H.A.: *Phys. Rev.* **57**, 1125–1144 (1940)
42. Miller, W.H., Morgner, H.: *J. Chem. Phys.* **67**, 4923–4930 (1977)
43. Brunetti, B., Candori, P., Falcinelli, S., Pirani, F., Vecchiocattivi, F.: *J. Chem. Phys.* **139**(16), 164305 (2013)
44. Falcinelli, S., Candori, P., Pirani, F., Vecchiocattivi, F.: *Phys. Chem. Chem. Phys.* **19**(10), 6933–6944 (2017)
45. Falcinelli, S., Rosi, M., Vecchiocattivi, F., Pirani, F.: Analytical potential energy formulation for a new theoretical approach in penning ionization. In: Misra, S., et al. (eds.) ICCSA 2019. LNCS, vol. 11621, pp. 291–305. Springer, Cham (2019). [https://doi.org/10.1007/978-3-030-24302-9\\_21](https://doi.org/10.1007/978-3-030-24302-9_21)
46. Brunetti, B., Candori, P., Falcinelli, S., Lescop, B., et al.: *Eur. Phys. J. D* **38**(1), 21–27 (2006)
47. Brunetti, B., Candori, P., De Andres, J., Pirani, F., Rosi, M., et al.: *J. Phys. Chem. A* **101**(41), 7505–7512 (1997)
48. Alagia, M., Boustimi, M., Brunetti, B.G., Candori, P., et al.: *J. Chem. Phys.* **117**(3), 1098–1102 (2002)
49. Alagia, M., Candori, P., Falcinelli, S., Mundim, M.S.P., Pirani, F., et al.: *J. Chem. Phys.* **135**(14), 144304 (2011)
50. Alagia, M., Bodo, E., Decleva, P., Falcinelli, S., et al.: *Phys. Chem. Chem. Phys.* **15**(4), 1310–1318 (2013)
51. Pirani, F., Maciel, G.S., Cappelletti, D., Aquilanti, V.: *Int. Rev. Phys. Chem.* **25**, 165–199 (2006)
52. Candori, P., Falcinelli, S., Pirani, F., Tarantelli, F., Vecchiocattivi, F.: *Chem. Phys. Lett.* **436**, 322–326 (2007)
53. Falcinelli, S., Vecchiocattivi, F., Pirani, F.: *Commun. Chem.* **3**(1), 64 (2020)
54. Gordon, S.D.S., Omiste, J.J., Zou, J., Tanteri, S., Brumer, P., Osterwalder, A.: *Nat. Chem.* **10**, 1190–1195 (2018)
55. Gordon, S.D.S., Zou, J., Tanteri, S., Jankunas, J., Osterwalder, A.: *Phys. Rev. Lett.* **119**, 053001 (2017)
56. Gregor, R.W., Siska, P.E.: *J. Chem. Phys.* **74**, 1078–1092 (1981)
57. Skouteris, D., Balucani, N., Faginas-Lago, N., et al.: *A&A* **584**, A76 (2015)
58. Skouteris, D., Balucani, N., Ceccarelli, C., Faginas Lago, N., et al.: *MNRAS* **482**, 3567–3575 (2019)
59. Jankunas, J., Bertsche, B., Jachymski, K., Hapka, M., Osterwalder, A.: *J. Chem. Phys.* **140**, 244302 (2014)